



**HAL**  
open science

# A novel lattice-based model for investigating three-dimensional fungal growth on solid media

Huan Du, Patrick Perre

► **To cite this version:**

Huan Du, Patrick Perre. A novel lattice-based model for investigating three-dimensional fungal growth on solid media. *Physica A: Statistical Mechanics and its Applications*, 2020, 541, pp.123536. 10.1016/j.physa.2019.123536 . hal-03140194

**HAL Id: hal-03140194**

**<https://hal.science/hal-03140194>**

Submitted on 21 Jul 2022

**HAL** is a multi-disciplinary open access archive for the deposit and dissemination of scientific research documents, whether they are published or not. The documents may come from teaching and research institutions in France or abroad, or from public or private research centers.

L'archive ouverte pluridisciplinaire **HAL**, est destinée au dépôt et à la diffusion de documents scientifiques de niveau recherche, publiés ou non, émanant des établissements d'enseignement et de recherche français ou étrangers, des laboratoires publics ou privés.



Distributed under a Creative Commons Attribution - NonCommercial 4.0 International License

# A novel lattice-based model for investigating three-dimensional fungal growth on solid media

Huan Du<sup>a,b,c</sup>, Patrick Perré<sup>c,d</sup>

<sup>a</sup>*Institute for Advanced Study, Shenzhen University, Shenzhen 518060, China*

<sup>b</sup>*College of Physics and Optoelectronic Engineering, Shenzhen University, Shenzhen 518060, China*

<sup>c</sup>*LGPM, CentraleSupélec, SFR Condorcet FR CNRS 3417, Université Paris-Saclay, Centre Européen de Biotechnologie et de Bioéconomie (CEBB), 3 Rue des Rouges Terres, 51110, Pomacle, France*

<sup>d</sup>*LGPM, CentraleSupélec, Université Paris-Saclay, 8-10 Rue Joliot-Curie, 91190, Gif-sur-Yvette, France*

---

## Abstract

Filamentous fungi can regulate their growth mechanisms to adapt to the environment and form different morphologies. On solid media, their first action is generally to adhere to a surface and form an approximately planar shape on a flat substrate. In a three-dimensional (3D) modelling approach, this environment is therefore heterogeneous along the z-direction. To clarify the interactions between hyphal behaviours and this heterogeneous environment, a 3D discrete model was developed. This model applied a special lattice-based approach which eliminates the restriction of lattice configuration to the simulated mycelia networks while maintaining high computational efficiency. It incorporates explicitly the mechanisms of hyphal elongation, apical and lateral branching, anastomosis and tropism, and is rigorously validated by the experimental data on *Postia placenta* growth on malt extract agar. Results compared with experimental data showed that the presence of substrate at  $z = 0$  bends the extension direction of hyphae towards the substrate surface. To mimic the experimental data, the bending rate was determined by an exponential-like tropism. Moreover, the branching direction was also constrained on the stage of its emergence. Compared to a simpler 2D model, the simulations of the 3D model were closer to actual growth, hence leading to a realistic mycelial network in terms of both configuration and biomass density. This 3D model can be easily extended to investigate fungal growth in other scenarios, such as for solid-state fermentation in incorporating hyphal penetration, in obstructed environments and even in wood panels.

**Keywords:** Mycelium, lattice-based, tropism, three-dimensional modelling, heterogeneous media, *Postia placenta*

---

\*Patrick Perré

*Email address:* [patrick.perre@centralesupelec.fr](mailto:patrick.perre@centralesupelec.fr) (Patrick Perré)

## 1. Introduction

Filamentous fungi can grow and survive in diverse habitats due to their highly-branched and interconnected networks. It has been proposed that hyphae can sense and then adapt their growth dynamics to the surroundings [1, 2, 3, 4]. Thus, different morphologies of mycelium are formed depending on their growth environments. For example, fungal mycelia can form spherical pellets in submerged culture as well as biofilms adhering to solid substrate surfaces [5]. The mycelial growth on flat substrates is approximately planar since it tends to more likely enlarge its surface in the xy-plane than its thickness in the z-direction. At the first phase of growth, the mycelia generate a high density of hyphae to form a random network with a minuscule height above the surface [6]. To investigate how hyphae behave to form this dense layer, a mathematical modelling method was applied to simultaneously capture the mycelial morphology and biomass development in three-dimensional (3D) space, in analysing the tropism produced by heterogeneity in the z-direction which has been proved difficult in experimental studies.

The discrete modelling approach is generally applied to studying the behaviours of individual hyphae and describing the morphology of mycelia. Two methods are widely used in deriving discrete models of mycelial growth. In the lattice-free models, the mycelial networks are represented by a collection of connected line segments with no restrictions on the position of these segments [7, 8, 9, 10, 11, 12, 13, 14]. These models can generate networks closely resembling realistic mycelia, which allows for assessment of hyphal growth at the individual level and hence improved understanding of interactions between hyphal behaviours and the environment. However, the computational complexity is generally high and some mechanisms, such as lateral branching or anastomosis, are too complex to be incorporated. In contrast to the lattice-free approach, lattice-based modelling is confined to a regular lattice used as the geometrical basis for developing the mycelial network by formulating a series of stochastic rules applied on the nodes of the lattice [15, 16, 17, 18, 19]. Due to the presence of a regular lattice with a finite number of status transition rules, complex behaviours of hyphae can be modelled while significantly improving computational efficiency. However, the artificial and predefined lattice greatly constrains the topology of the mycelial network leading to an unrealistic morphology.

Thus far, few of those models have been rigorously validated and none can simultaneously generate realistic mycelial morphology and predict biomass growth. In the biotechnology and construction industries, the estimation of fungal biomass is essential to improve the production or protection processes. As it is difficult to separate mycelia from solid substrates, the measurement of biomass by experimental approaches is labour-intensive and time-consuming [20]. Thus, a model with predictive capacity could be an efficient tool to help understand and improve these processes.

In this paper, a model was developed incorporating the main hyphal behaviours,

45 including hyphal elongation, apical and lateral branching, anastomosis and tropism,  
in a cubic lattice to simulate the mycelial network in the 3D space. A novel algo-  
rithm developed to simulate the elongation mechanism removed the restriction of the  
lattice configuration to the hyphal extension direction, and hence allowed the gener-  
ation of highly-realistic mycelia while maintaining high computational efficiency.  
50 This work focuses on simulating the 3D mycelial growth on a flat substrate to inves-  
tigate dense hyphae layer formation. The simulation results allowed us to observe  
that both the hyphal elongation direction and the emerging direction of branches are  
affected by this environment. The model was rigorously validated by experimental  
growth data of *Postia placenta* [21]. Model parameter estimation fully considered  
55 biological uncertainties in the form of probability distributions instead of fixed val-  
ues. This statistical approach is increasingly considered a necessary feature instead  
of a weakness for microbial systems [22]. The high correlation between the simulated  
and experimental results confirms the predictive capacity of this model in terms of  
both spatio-temporal biomass evolution and morphology. Moreover, this model can  
60 be easily extended to other applications and we provided three examples in the last  
section: hyphal penetration into solid media, bent growth in an obstructed environ-  
ment and fungal development in fibreboard.

## 2. Modeling

65 In this model, the space is discretised by a 3D cubic lattice with a side length of  $\delta$ .  
Each node  $(x_i, y_j, z_k)$  in the lattice has two potential statuses, either vacant or occu-  
pied by a hypha. Hyphal tips locate in their corresponding nodes and are defined by  
three variables:  $O(i, t)$ ,  $\vec{n}(i, t)$  and  $R(i, t)$  which denote respectively the location, the  
tip growth direction and the extension rate of tip  $i$  at time  $t$ . Since the elongation of a  
70 hypha occurs only at its tip, each hypha consists of a set of linked nodes which are the  
time-sequence of the previous tip positions in the model. The three main behaviours  
of mycelial growth, hyphal elongation, apical and lateral branching and anastomo-  
sis, and the response of hyphal tips to environmental stimuli are implemented into  
the 3D cubic lattice. These biological behaviours of hyphae are illustrated in Table 1.

75

### 2.1. Hyphal elongation

Without external stimuli, hyphal elongation proceeds in a relatively straight di-  
rection with frequent meandering for most fungi. From time to time, hyphae abandon  
the original growth direction and establish a new one with a minor directional change  
80 of approximately  $10^\circ$  due to the shift Spitzenkörper trajectory [24]. To model the  
hyphal elongation, a unit vector  $\vec{n}$  is determined to represent the tip extension di-  
rection. At each time step, the tip can advance into one of the three neighbouring  
nodes adjacent to this direction, respectively along the x-, y- and z-axis, as shown in

Table 1. Illustration of fungal growth behaviors [23].

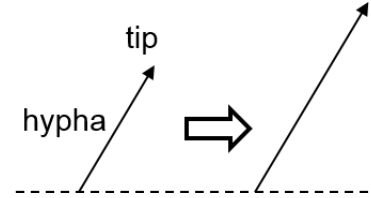
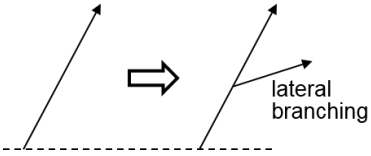
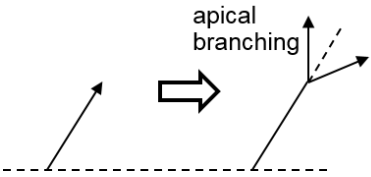
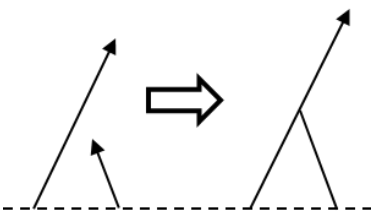
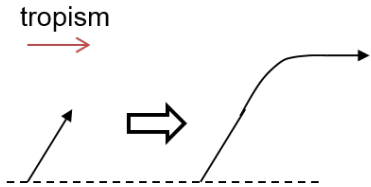
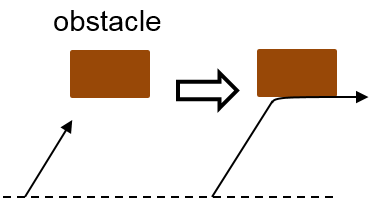
| Growth Behavior   | Growth Pattern   |
|-------------------|--|
| Hyphal elongation |    |
| Lateral branching |    |
| Apical branching  |    |
| Anastomosis       |  |
| Tropism           |  |
| Obstacle          |  |

Fig. 1(A)I, or remain in its actual position according to the probabilities as follows:

$$\begin{cases} P_x(i, t) = \frac{\tau}{\delta} R(i, t) \vec{n}(i, t) \cdot \vec{e}_x, \\ P_y(i, t) = \frac{\tau}{\delta} R(i, t) \vec{n}(i, t) \cdot \vec{e}_y, \\ P_z(i, t) = \frac{\tau}{\delta} R(i, t) \vec{n}(i, t) \cdot \vec{e}_z, \\ P_{none}(i, t) = 1 - [P_x(i, t) + P_y(i, t) + P_z(i, t)], \end{cases} \quad (1)$$

85 where  $\tau$  is the duration of each time step;  $\vec{e}_x$ ,  $\vec{e}_y$  and  $\vec{e}_z$  are the standard basis for the 3D Euclidean space. The probability of the movement into the other three nodes is consequently set to be zero. After several iterations, the successive biased random walks of the tip form a pathway globally along the elongation direction (Fig. 1(A)II). Note that if the tip extension rate  $R > 0$ , the tip is active and if  $R = 0$ , the tip is  
90 dormant and does not elongate.

As hyphae change their growth axis periodically, the tip extension direction is updated with probability  $P_{dir}$  to decide whether a small directional change occurs or not. When it happens, the direction varies by  $10^\circ$  with respect to its former di-  
95 rection. Since all the satisfied vectors constitute a conical surface around the former direction vector, one of them is selected randomly.

## 2.2. Branching

Hyphae generate new tips by branching, of which two types, apical and lat-  
100 eral branching, are defined according to their emerging sites and their growth patterns [25]. Apical branching occurs at hyphal tips and divides one tip into two which develop symmetrically around the original tip. Lateral branches emerge from the sub-apical part of one hypha. According to statistical analysis, the selection of lat-  
105 eral/apical branch sites is almost equiprobable throughout the whole mycelium/tips independent of the hyphal age or the branch density [21, 23]. However, it is observed that the proximity of a hyphal tip or an existing branch inhibits the emergence of a new lateral branch [26].

In this model, a probability  $P_b^l$  is defined to determine the frequency of lateral branching during a time step. The number of lateral branches to be formed at time  
110  $t$  is calculated as follows:

$$\Delta N_b^l(t) = N_b^l(t) - N_b^l(t - \tau) = \lfloor P_b^l N_p(t) \rfloor + 1_{A1}(\omega) \quad (2)$$

where  $N_p(t)$  is the total number of tips at time  $t$ ; " $\lfloor \cdot \rfloor$ " a floor function mapping the real number to the largest previous integer;  $1_{A1}$  an indicator function which has the value 1 if  $\omega \in A1$ ;  $\omega$  a number randomly picked in the interval  $[0, 1]$ ;  $A1 = \{x | x \in (0, P_b^l N_p(t) - \lfloor P_b^l N_p(t) \rfloor)\}$ . The  $\Delta N_b^l$  positions of branch emergence are  
115 randomly selected from the set involving all the nodes occupied by hyphae except those that have already emerged branches. In addition, one node is also considered inhibited either by apical dominance when the distance of this node to the tip is less than  $l_{ad}$ , or by an adjacent existing branch when the distance of this node to the

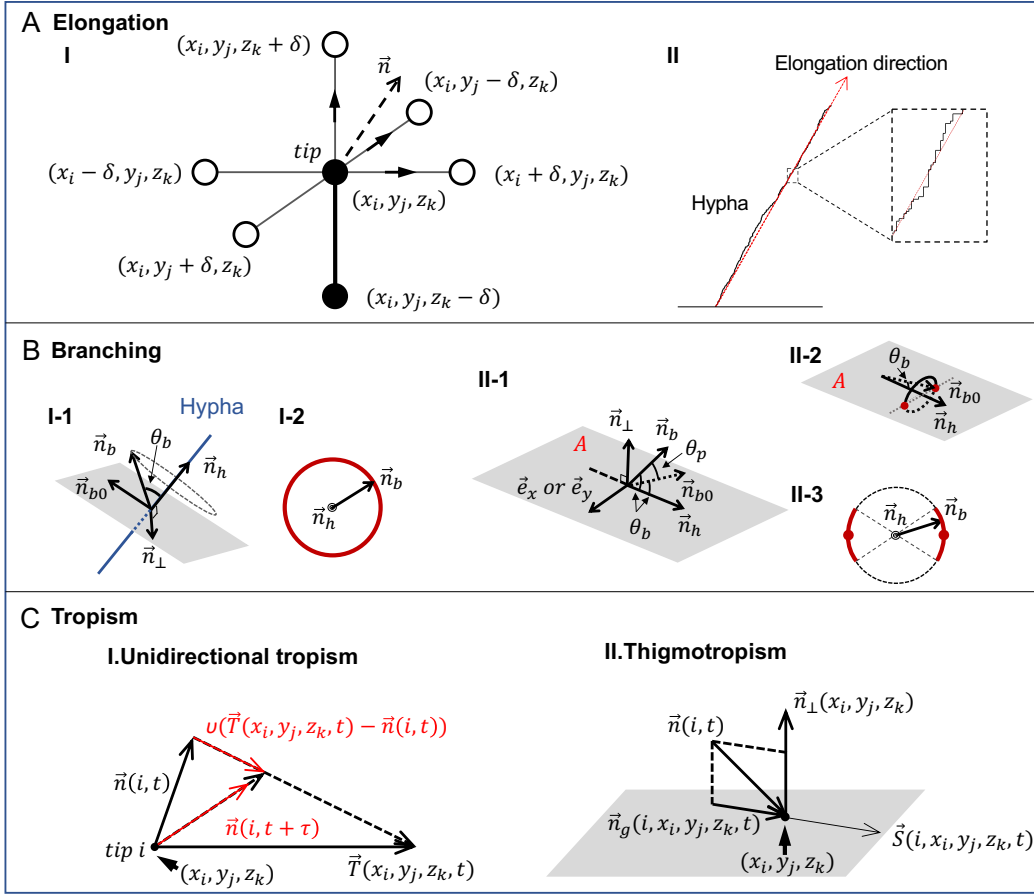


**Fig. 1. Main mechanisms of hyphal growth.** (A)I Hyphal elongation rules: consider the tip at location  $(x_i, y_j, z_k)$  and the six nodes adjacent to it; tip movement with  $P_x$ ,  $P_y$  and  $P_z$  to select randomly one of the three nodes,  $(x_i + \delta, y_j, z_k)$ ,  $(x_i, y_j - \delta, z_k)$  and  $(x_i, y_j, z_k + \delta)$ , adjacent to the tip extension direction identified by  $\vec{n}$ , as the target node during the next time step. (A)II The global shape as an emergence of the local rules: after many iterations, the successive movements of the tip form a pathway globally along the elongation direction. (B)I Free branching: the emerging direction is a vector  $\vec{n}_b$  randomly selected among the cone having the angle  $\theta_b$  with the hyphal direction  $\vec{n}_h$ . All positions of the circle of unit length of this cone (red circle of the figure) are equiprobable. (B)II Constrained branching: the emerging direction is selected from two arcs of this unit length circle. These arcs (red curve) range over an angle  $\pm\sigma_p$  around the two intersection points (red points) between this circle and the plane span by the tip direction  $\vec{n}_h$  and its orthogonal direction belonging to the substrate plane. (C)I Unidirectional tropisms: the updated tip extension direction for the next time step  $\vec{n}(i, t + \tau)$  is obtained by applying the unidirectional tropism  $\vec{T}$  to  $\vec{n}(i, t)$ ;  $v$  is the reaction rate of hyphae. (C)II Thigmotropism: calculation of the thigmotropism  $\vec{S}$  applied to the tip  $i$  located at  $(x_i, y_j, z_k)$  at time  $t$ ;  $\vec{n}_\perp$  is the unit normal vector of the solid surface,  $\vec{n}$  denotes the tip extension direction, and  $\vec{n}_g$  is the vector projection of  $\vec{n}$  on the tangent of the solid surface.

branch is less than  $l_{nabr}$ .

120

Since the apical branching occurs at the active tips, a probability  $P_b^a$  is applied to all active tips, then the number of apical branching during the time increment is

obtained as follows:

$$\Delta N_b^a(t) = N_b^a(t) - N_b^a(t - \tau) = \lfloor P_b^a N_{ap}(t) \rfloor + 1_{A2}(\omega) \quad (3)$$

where  $N_{ap}(t)$  is the total number of active tips ( $R > 0$ ) at time  $t$ ;  $1_{A2}$  an indicator  
 125 function which has the value 1 if  $\omega \in A2$ ;  $\omega$  a random number in the interval  $[0, 1]$ ;  
 $A2 = \{x | x \in (0, P_b^a N_{ap}(t) - \lfloor P_b^a N_{ap}(t) \rfloor)\}$ .  $\Delta N_b^a(t)$  tips are randomly selected from  
 all active tips.

After selection of the branch sites, the emerging direction of the new branches  
 130 should be determined. A basic method is constructed to simulate the free emergence  
 of branches in 3D space as shown in Fig. 1(B)I. Then, according to observation of  
*Postia placenta* growth on solid media, hyphae are likely to extend initially along  
 the surface to cover it. Therefore, a constrained method is established to lead the  
 emerging branches with a direction approaching or along the surface.

### 135 2.2.1. Free branching

The tangent direction to a hypha at a node  $(x_i, y_j, z_k)$  is determined by a unit  
 vector  $\vec{n}_h = (x, y, z)$  and is equal to the tip extension direction when the tip was at  
 this position. The extension direction of a lateral branch emerging from the node  
 $(x_i, y_j, z_k)$  forms an angle of  $\theta_b$ , which is named the branching angle determined as  
 140 a normal distribution, with  $\vec{n}_h$ . As shown in Fig. 1(B)I-1, in 3D space, all of the  
 possible directions  $\vec{n}_b$  form a cone. To randomly select one vector from the cone, two  
 intermediate vectors,  $\vec{n}_\perp$  and  $\vec{n}_{b0}$ , should be calculated. First, the vector  $\vec{n}_\perp$ , which  
 is located in the plane perpendicular to  $\vec{n}_h$ , is determined as follows:

$$\vec{n}_\perp = -a\sqrt{\frac{1}{1-a^2}}\vec{n}_h + \sqrt{\frac{1}{1-a^2}}\vec{a}, \quad (4)$$

where  $\vec{a} = (x, 0, 0)$  if  $|x| \leq |y| \leq |z|$  and so forth. Then, an angle  $\theta$  is randomly  
 145 selected from the interval  $[0, 2\pi]$  to identify the vector  $\vec{n}_{b0}$  which is also located in  
 the perpendicular plane but at an angle of  $\theta$  to  $\vec{n}_\perp$  (Fig. 1(B)I-2):

$$\vec{n}_{b0} = \cos \theta \vec{n}_\perp + \sin \theta (\vec{n}_h \wedge \vec{n}_\perp). \quad (5)$$

Finally, the emerging direction of the new branch denoted by  $\vec{n}_b$  (Fig. 1(B)I-3) is  
 calculated as the vector simultaneously in the cone and in the plane determined by  
 $\vec{n}_h$  and  $\vec{n}_{b0}$  by the following expression:

$$\vec{n}_b = \cos \theta_b \vec{n}_h + \sin \theta_b \vec{n}_{b0}. \quad (6)$$

150 For the apical branching, the same method is applied using the extension direction  
 of that tip  $\vec{n}$  instead of  $\vec{n}_h$ . After the determination of the emerging direction of one  
 branch denoted by  $\vec{n}_{b1}$ , the other one denoted by  $\vec{n}_{b2}$  can be calculated with  $\vec{n}_{b1}$  and  
 $\vec{n}$  (Eq. 7), since the two new branches are symmetrical with respect to the previous  
 tip direction.

$$\vec{n}_{b2} = 2 \cdot (\vec{n} \cdot \vec{n}_{b1}) \cdot \vec{n} - \vec{n}_{b1}. \quad (7)$$



155 *2.2.2. Constrained branching*

As shown in Fig. 1(B)II, the objective is to limit the emerging direction of branching to a small band around the plane  $A$  determined by the direction of the mother hypha  $\vec{n}_h = (x, y, z)$  and the unit vector  $\vec{e}_x$  or  $\vec{e}_y$ . More specifically, the branching direction  $\vec{n}_b$  is no more randomly selected among all the possible directions which constitute a cone around  $\vec{n}_h$ , but is determined by an amplitude angle  $\theta_p$  which is determined as a normal distribution  $\theta_p \sim \mathcal{N}(0^\circ, \sigma_p)$  (Fig. 1(B)II-2,3). To determine  $\vec{n}_b$ , firstly, the normal vector  $\vec{n}_\perp$  of the plane  $A$  determined by  $\vec{n}_h$  and  $\vec{a}$  is calculated by the equations:

$$\begin{cases} \vec{n}_\perp \cdot \vec{n}_h = 0, \\ \vec{n}_\perp \cdot \vec{a} = 0, \\ \|\vec{n}_\perp\| = 1. \end{cases} \quad (8)$$

where  $\vec{a} = \vec{e}_x$  if  $|x| \leq |y|$  and  $\vec{a} = \vec{e}_y$  if not. Then, the intersected vector  $\vec{n}_{b0}$  of the plane  $A$  and the cone constituting all possible branching directions is determined as follows:

$$\begin{cases} \vec{n}_{b0} \cdot \vec{n}_h = \|\vec{n}_{b0}\| \cdot \|\vec{n}_h\| \cdot \cos \theta_b, \\ \vec{n}_{b0} \cdot \vec{n}_\perp = 0, \\ \|\vec{n}_{b0}\| = 1. \end{cases} \quad (9)$$

Finally, the branching direction  $\vec{n}_b$  is calculated with an amplitude angle  $\theta_p$  between it and  $\vec{n}_{b0}$ :

$$\begin{cases} \vec{n}_b \cdot \vec{n}_h = \|\vec{n}_b\| \cdot \|\vec{n}_h\| \cdot \cos \theta_b, \\ \vec{n}_b \cdot \vec{n}_{b0} = \|\vec{n}_b\| \cdot \|\vec{n}_{b0}\| \cdot \cos \theta_p, \\ \|\vec{n}_b\| = 1. \end{cases} \quad (10)$$

To calculate the apical branching direction, the same method is applied using the tip direction  $\vec{n}$  instead of  $\vec{n}_h$ .

170 *2.3. Anastomosis*

Anastomosis is the fusion between two hyphae in contact with each other to yield an interconnected mycelial network [27]. The advantage is to facilitate communication and translocation among hyphae. This mechanism is simply incorporated in the model by assuming that it occurs when a hyphal tip contacts another hypha. After the fusion, the tip no longer exists.

*2.4. Tropisms*

Hyphal growth, particularly growth direction, responds to environmental stimuli, [28, 4, 3, 29, 30]. In considering the environmental features, two types of tropisms are incorporated into this model, unidirectional tropism and thigmotropism. The unidirectional tropism leads the growth of hyphae more or less rapidly in one direction

which is determined by the location of the stimuli, while the thigmotropism makes hyphae elongate along or bend around the surface of obstacles.

185 As shown in Fig. 1(C)I, the unidirectional tropism is represented by a vector field  $\vec{T}(x_i, y_j, z_k, t)$  of which the magnitude represents the intensity of this tropism. In addition to the tropism intensity, different species may have different reaction rates so that a coefficient of hyphal reaction rate  $v$  is defined. The tip extension direction  $\vec{n}$  is changed by the tropism  $\vec{T}$  at each time step as follows:

$$\begin{aligned}\vec{n}(i, t + \tau) &= \frac{\vec{n}(i, t) + \Delta\vec{n}(i, t)}{\|\vec{n}(i, t) + \Delta\vec{n}(i, t)\|}, \\ \Delta\vec{n}(i, t) &= v[\vec{T}(x_i, y_j, z_k, t) - \vec{n}(i, t)].\end{aligned}\tag{11}$$

190 The thigmotropism  $\vec{S}(i, x_i, y_j, z_k, t)$  is related to both the presence of solids and the direction of tips. As shown in Fig 1(C)II, the direction of the thigmotropism is within the plane tangent to the surface. The intensity of this tropism depends on the extension direction of the tip  $i$  arriving at  $(x_i, y_j, z_k)$  (i.e.,  $\vec{n}(i, t)$ ) and the intensity coefficient  $c_s(x_i, y_j, z_k)$  with  $c_s > 0$  for the nodes surrounding the solids and  $c_s = 0$  for the others. The thigmotropism vector is calculated as follows:

$$\begin{aligned}\vec{S}(i, x_i, y_j, z_k, t) &= c_s(x_i, y_j, z_k) \frac{\vec{n}_g(i, x_i, y_j, z_k, t)}{\|\vec{n}_g(i, x_i, y_j, z_k, t)\|^2} \\ \vec{n}_g(i, x_i, y_j, z_k, t) &= \vec{n}(i, t) - [\vec{n}(i, t) \cdot \vec{n}_\perp(x_i, y_j, z_k)] \vec{n}_\perp(x_i, y_j, z_k)\end{aligned}\tag{12}$$

where  $\vec{n}_\perp$  is the normal vector of the surface at the point  $(x_i, y_j, z_k)$  and  $\vec{n}_g$  is the projection of the tip direction vector on the tangent plane. Due to the divisor  $\|\vec{n}_g\|^2$  in Eq. 12, the intensity of the thigmotropism decreases as the tip direction is getting closer to the plane of the surface. Since Eq. 11 is linear, this equation can be simply applied with the total tropism  $\vec{T}_{tot}$  obtained by the sum of tropisms (i.e.  $\vec{T}_{tot} = \vec{T} + \vec{S}$ ).

## 2.5. Calibration

This model was calibrated for the growth of *P. Placenta* on malt extract agar via our 2D model [23] which has been validated by experimental observation [21]. Most parameters adopt directly the values determined in the 2D model, while some, such as the branching probabilities, are obtained by Eq. 13 in rescaling their values. In Eq. 13,  $P$  denotes the probability,  $\tau$  is the time step, and the subscripts 3D and 2D represent the parameter value, respectively, in the 3D and 2D models. The time step  $\tau_{2D}$  is 1.5 min and  $\tau_{3D}$  is set as 1.3 min, as calculated by Eq. 14 where  $\delta = 3 \mu m$  and  $R_{max} = 80 \mu m/h$ . The lattice spacing  $\delta = 3$  is set as the average diameter of hyphae of *P. Placenta*. This constraint is required to incorporate the initial inoculum into the lattice and to compare the simulated and observed results, namely in terms of mass density. The active tips are selected from all active and dormant tips by a proportion  $P_{active} = 70\%$  just as in the 2D model. The description and the value of

215 the principal parameters are listed in table 2.

$$P_{3D} = P_{2D} \frac{\tau_{3D}}{\tau_{2D}}. \quad (13)$$

$$\tau \leq \frac{\delta}{\sqrt{3}R_{max}}. \quad (14)$$

**Table 2. Description and values of the principal modeling parameters [23].**

| Parameter      | Description                               | Value  |
|----------------|---|--|
| $\tau$         | Duration of time step                     | 1.3 min  |
| $\delta$       | Lattice spacing                           | 3 $\mu m$  |
| $R$            | Tip extension rate distribution           | $F'_\Gamma(R; \alpha, \beta) = F_\Gamma(\alpha = 1.51, \beta = 0.09) + 4.65 \times 10^{-6}(R_{max}R - \frac{1}{2}R^2)(R_{max} = 1.33\mu m min^{-1})$ |
| $P_{active}$   | Probability of tip activation             | 70%  |
| $\theta_b$     | Branching angle                           | $\mathcal{N}(\mu = 77.6^\circ, \sigma = 12.3^\circ)$   |
| $l_{ad}$       | Length of apical dominance                | 5 $\mu m$  |
| $l_{nobr}$     | Length of inhibition of lateral branching | 10 $\mu m$   |
| $P_{br}^{lat}$ | Probability of lateral branching          | $8.7 \times 10^{-4}$   |
| $P_{br}^{api}$ | Probability of apical branching           | $2.5 \times 10^{-4}$   |
| $P_{dir}$      | Probability of variation of tip direction | 0.01   |

### 2.6. Initial field and simulation

To be consistent with the experimental observation, the dimension of the lattice in the following simulations is defined as  $12 mm \times 12 mm \times 0.6 mm$  in x-, y- and z-direction. A cylindrical inoculum of constant height ( 0.23 mm) and bottom base area ( 0.55 mm<sup>2</sup>) as the observed one is put on the bottom surface of the lattice, in the centre of the xy-plane as the initial field (Fig.A1(A)). Only the nodes on the side of the cylinder can generate tips, and the initial tip direction is perpendicular to the z-axis and radially outward. The boundaries of the lattice are regarded as solid obstacles which engender thigmotropism in the adjacent hyphae. The simulations have been executed respectively in applying the two branching mechanisms with or without incorporating the unidirectional tropism which forces the hyphal growth towards the substrate surface (i.e. the xy-plane at  $z_k = 0 \mu m$ ). For all the simulations, we assigned the value 0.001 and 100.0 to the two coefficients,  $v$  and  $c_s$  in the tropism mechanism (equations 11 and 12). Moreover, two formulations of the tropism have been tested :

$$\text{Constant tropism} \quad \vec{T}(z_k) = -a\vec{e}_z, \quad (15)$$

$$\text{Exponential tropism} \quad \vec{T}(z_k) = -a(e^{z_k/h_0} - 1)\vec{e}_z, \quad (16)$$

where  $a$  and  $h_0$  are two constants. An example of simulation in applying the constrained branching and exponential tropism mechanisms is shown in Fig.A1(B).

### 3. Results and discussion

#### 3.1. Validation for mycelial growth on a flat medium

235 We first compared the profiles in the  $xz$ -plane of the simulated results with the column-averaged hyphal density of the 12-day-old experimental mycelium observed using confocal microscopy (CLSM) [21]. Four simulations were carried out in different combinations of two conditions: (i) free or constrained branching mechanisms and (ii) application of the tropism or not. As reported by the simulation results, 240 without tropism, the mycelium expanded in all directions, even though the branching direction was constrained (Fig.2(B)(C)). This is obvious for the free growth as no limits were imposed on the hyphal growth direction as shown in the zoom of Fig.2(B). When the hyphal direction is constrained (zoom of Fig.2(C)), after a long-term growth, the mycelium eventually expanded upwards, although this expansion 245 is much slower than for the free growth. However, the mycelium tended to cling to the substrate surface (Fig.2(A)). To force the hyphae to develop near the substrate surface, a downward tropism was applied (Fig.2(D)(E)). Nevertheless, since hyphae grew along all directions without constraints on the branching, those growing upwards were bent by the tropism, producing an unrealistic morphology, as shown in 250 the zoom of Fig.2(D). In conclusion, both the tropism and the constrained branching mechanism are essential to reproduce the mycelial growth on agar. It is notable that in 3D space, the medium is highly non-uniform in the  $z$ -direction. This implies that for the real development of mycelia, this spatial variation generates a tropism for hyphal elongation direction and simultaneously affects the branching mechanism to 255 adapt to this environment. The tropism may be explained by the need for water and nutrients for the mycelial growth, while the new branches should account for the presence of the substrate from the emergence phase.

In order to better understand the combined effects of tropism and constrained angle, a constant tropism was tested first (tropism value independent of  $z$ ). As 260 shown in Fig. 3(A), the 12-day-old mycelium observed using confocal microscopy was mapped into a 2D projection image and divided into a series of rings, of which the gap was  $\Delta r = 60 \mu m$ . The normalized radial density of hyphal biomass denoted by  $\rho(r)$  was calculated as the proportion of occupied pixels for each radius increment. 265 For the simulation results, one must keep in mind that a single realization contains fluctuations due to the numerous stochastic processes in the model. The simulated radial density  $B(r)$  is, therefore, the average over 50 simulations performed with the

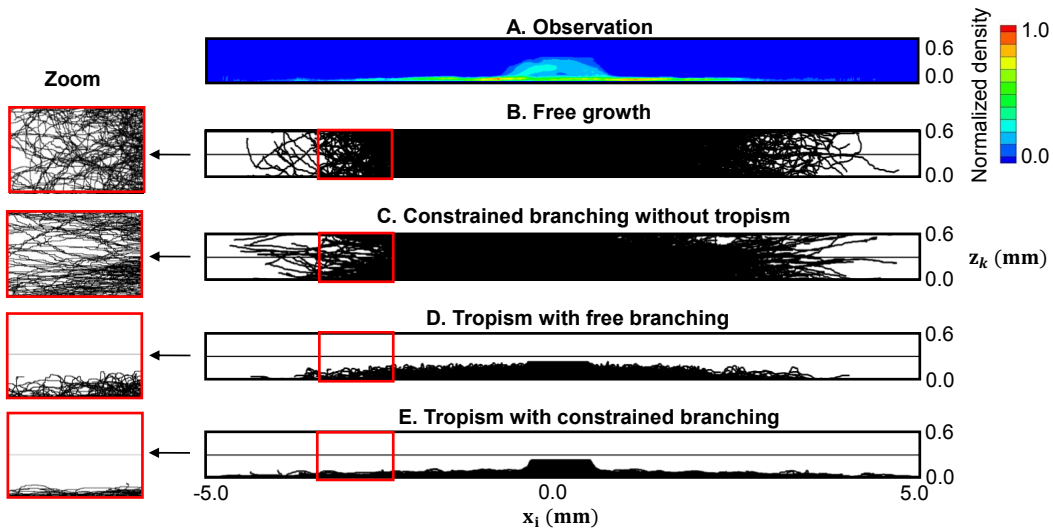


**Fig. 2. Simulated profiles in the  $xz$ -plane and column averaged hyphal density obtained by the experimental observation.** (A) Experimental result: the normalized column averaged hyphal density of the 12-day-old mycelium. Simulation results in applying: (B) Free branching mechanism without tropism; (C) Constrained branching mechanism ( $\theta_p \sim \mathcal{N}(0^\circ, 3^\circ)$ ) without tropism; (D) Exponential tropism ( $\vec{T} = -1.0(e^{z_k/45.0} - 1)\vec{e}_z$ ) with free branching mechanism; (E) Exponential tropism ( $\vec{T} = -1.0(e^{z_k/45.0} - 1)\vec{e}_z$ ) with constrained branching mechanism ( $\theta_p \sim \mathcal{N}(0^\circ, 3^\circ)$ ).

same parameters. As shown in Fig. 3(B), when the tropism intensity  $\|\vec{T}\| = 2.0$ , the simulated density of the marginal part of the colony approximates with the observed density, but not for the central part. If we increased the tropism intensity to reduce the density in the center, the hyphae in the marginal part would also be largely decreased. According to these curves, a strong tropism is required to drive the hyphae far away from the agar surface to quickly grow downwards, while the marginal part needs only a relatively weak tropism to maintain a certain colony thickness. The tropism intensity must, therefore, depend on the distance between the hyphae and the agar surface. Hence, a method was established to estimate the tropism for identifying the averaged  $z$ -position of hyphae and the necessary tropism intensity respectively for the central and marginal parts.

As shown in Fig. 3(C-D), for the four different ranges of the branching amplitude angle  $\theta_p$  (presented in Eq.10), we tested numerous constant tropisms to make the simulated results correspond to the observed hyphal density either in the central part or in the marginal part. Among all the tested tropisms,  $\vec{T} = -30.0\vec{e}_z$  best fits the density in the central part for all the four angles, while for the marginal part, the tropism intensity augments from 0.5 to 2.5 with an increase of amplitude angles. When the tropism is low, the greater the range of the amplitude angle, and the higher the tropism needs to be to compensate. However, if the tropism is strong enough, the effect of the amplitude angle is negligible. After determination of the tropism intensity for the two parts, the corresponding  $z$ -position of hyphae were estimated by selecting three radii-points evenly distributed in each of the central and marginal

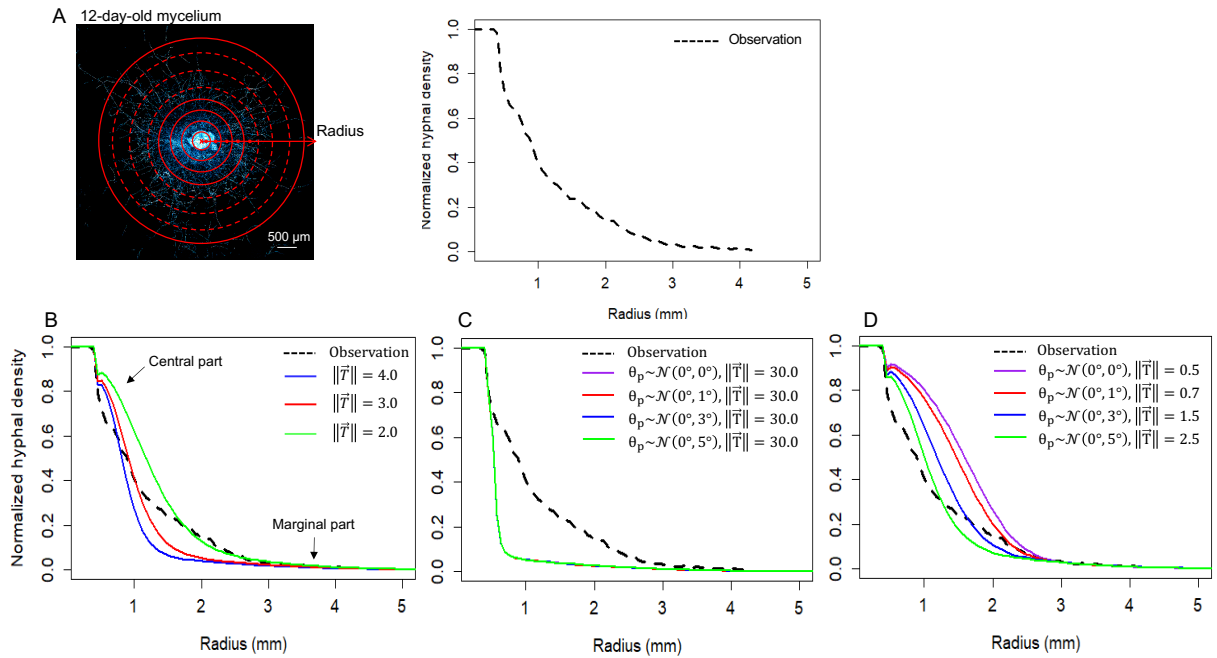


**Fig. 3. Normalized radial density of hyphae obtained from the experimental observation and simulations under constant tropisms.** Radial hyphal density of 12-day-old mycelium, observed (A) in the experiment (dashed line) and obtained by simulations: (B) in applying three constant tropisms respectively with the intensity of  $\|\vec{T}\| = 4.0, 3.0$  and  $2.0$ , and the constrained branching mechanism with  $\theta_p \sim \mathcal{N}(0^\circ, 3^\circ)$ ; in fitting the biomass density respectively (C) in the central part and (D) in the marginal part with different couples of range of amplitude angle and constant tropism  $(\theta_p, \vec{T})$ .

parts. Then, the thicknesses of the colony at these three radii were measured and averaged as the mean z-direction distance between hyphae and the substrate surface for the central (i.e.,  $160 \mu m$ ) and the marginal part (i.e.,  $50 \mu m$ ), respectively. Thus, an exponential equation (Eq. 15) for each amplitude angle was determined from the three points, the origin  $(0,0)$  and the two couples of  $(z_k, \|\vec{T}\|)$  (Fig. 4(A)). Theoretically, with a greater range of  $\theta_p$ , the space for hyphal growth enlarges and hence the biomass increases, especially for the marginal part. Accordingly, the tropism intensity should augment to compress the space enlarged by  $\theta_p$  just as shown in Fig. 4(A).

Simulations were performed with these couples of exponential tropisms and amplitude angles to determine how well they fit the experimental data. Results show that all combinations concurred with the observed results (Fig. 4(B-I)), except for a minor difference in the variation of the curve slope along the radius. For example, compared with  $\theta_p \sim \mathcal{N}(0^\circ, 0^\circ)$ , the curve steepness obtained in applying  $\theta_p \sim \mathcal{N}(0^\circ, 5^\circ)$  flattens faster with radius. The tropism over-compressed the biomass in the central part and insufficiently in the marginal part. The relative error between the simulated and observed results was calculated by Eq. 17, where  $\rho(r_k)$  and  $B(r_k)$  are respectively

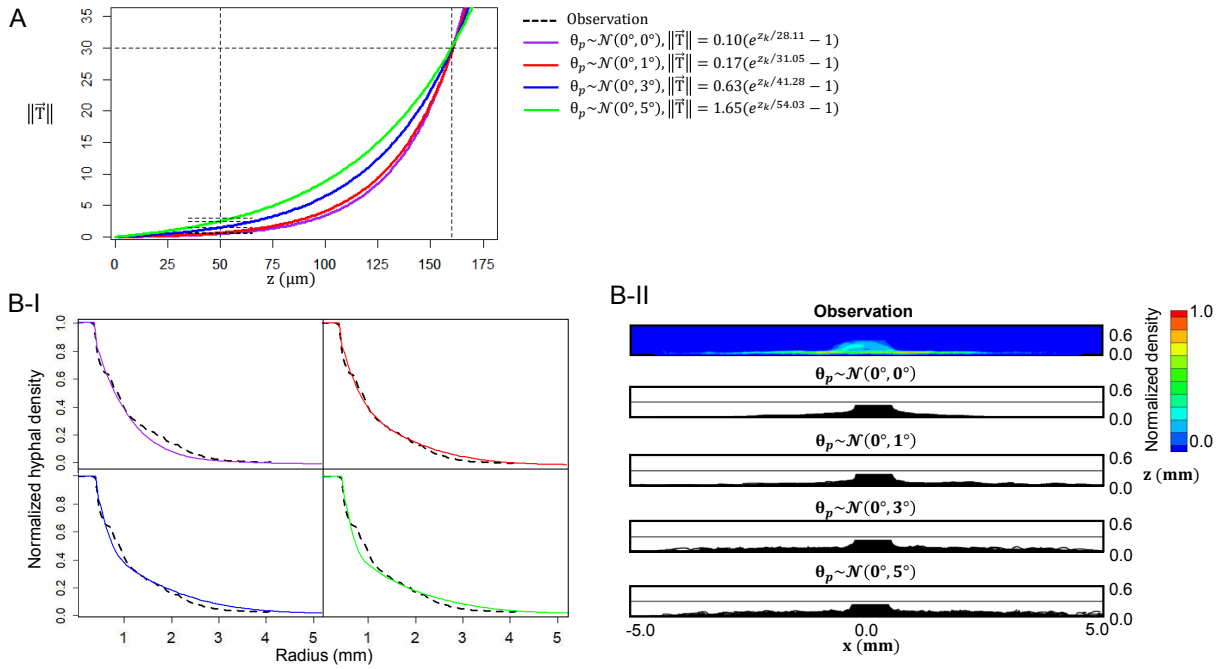


**Fig. 4. The simulated results under tropism for four ranges of branching amplitude angle compared with the experimental results.** (A) Exponential curves passing through the original point and the two points  $(z_k, \|\vec{T}\|)$ , respectively, identified for the central and marginal parts to determine the appropriate global tropism. ( $z_k$  - averaged distance between hyphae and the substrate surface,  $\|\vec{T}\|$  - corresponding constant tropism intensity.) Comparison of (B)-I the simulated radial densities and (B)-II the lateral profiles of the simulated mycelia in the  $xz$ -plane obtained in applying the four ranges of amplitude angle and their corresponding tropisms with the experimental results.

the observed and simulated radial density of biomass:

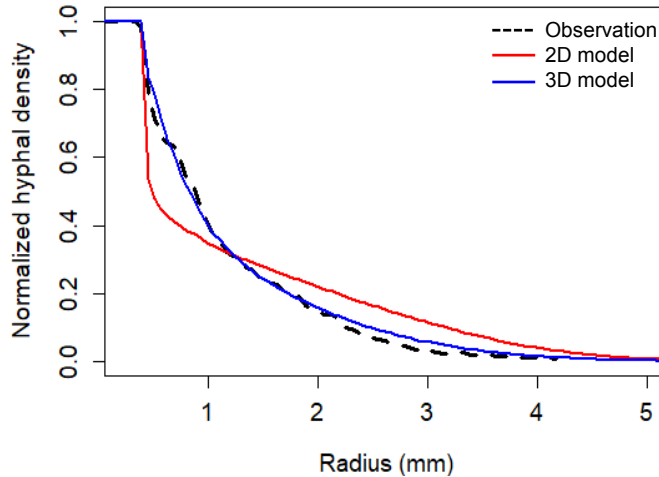
$$Error = \sqrt{\frac{\sum_{k=1}^N (\rho(r_k) - B(r_k))^2}{\sum_{k=1}^N \rho^2(r_k)}}. \quad (17)$$

By considering both the shape of the curves and the errors listed in Table 3, one can conclude that the most relevant simulation is obtained with  $\theta_p \sim \mathcal{N}(0^\circ, 1^\circ)$  and the corresponding tropism. This result is also confirmed by the  $xz$ -plane mycelium profiles shown in Fig. 4(B-II), which shows a variation of colony thickness with radius very similar to that of the experiment. This result implies that on a solid substrate, the mycelial growth mechanisms, including the hyphal elongation and the branching emergence, are established to force the hyphae to adhere to the substrate surface within a controlled deviation. According to the simulated results, the tropism is greater when the hyphae are further away from the surface and moreover, its reduction rate slows while the hyphae approach the surface to achieve a stable state.

**Table 3. Relative error between the observed and simulated density of biomass.**

| $\theta_p$                      | $\vec{T}$                           | Relative error |
|---------------------------------|-------------------------------------|----------------|
| $\mathcal{N}(0^\circ, 0^\circ)$ | $-0.10(e^{z_k/28.11} - 1)\vec{e}_z$ | 0.0814         |
| $\mathcal{N}(0^\circ, 1^\circ)$ | $-0.17(e^{z_k/31.05} - 1)\vec{e}_z$ | 0.0505         |
| $\mathcal{N}(0^\circ, 3^\circ)$ | $-0.63(e^{z_k/41.28} - 1)\vec{e}_z$ | 0.0785         |
| $\mathcal{N}(0^\circ, 5^\circ)$ | $-1.65(e^{z_k/54.03} - 1)\vec{e}_z$ | 0.0999         |

320 The 3D model better matches the observed results than our previous 2D model [23] as shown in Fig. 5. The 3D model is an improvement in terms of the replication of growth environments and the growth mechanisms of fungi. Hyphae are able to extend in the z-direction either for elongation or for branching. Moreover, anastomosis occurs in nature when two hyphae touch each other and therefore does not depend  
325 on a probability parameter such as that in the 2D model. In the 3D model, the occurrence of anastomosis relies on the local hyphal quantity and their actual occupied space, which is more reliable.

**Fig. 5. Comparison the simulated densities obtained by the 2D and 3D models with the experimental data.**

Finally, the evolution of the modelled mycelial colony over time was compared  
330 with the observed results at different time points (Fig. 6). The 3D model matches the data well at 7 and 12 days, but less so at 5 days. At first, the initial conditions supplied to the model were rather simple compared to the complexity of the real inoculum used in the experiment. In addition, the mycelium requires a certain time after inoculation to adapt to its environment. These two reasons explain why the simulated results poorly match the experimental data at the shortest growth times.  
335 As shown in Fig. 7, the mycelial network on the 5<sup>th</sup> day is denser in the simulation than in the experiment. Fig. 7 proposes a representation of the 3D morphology of fungal colonies. Accounting for the great variability of biological behaviours and the number of random processes existing in real mycelial growth as well as in the model,  
340 it is impossible to reproduce the same mycelial network. Nevertheless, this 3D model



derived from the individual hyphal behaviours is able to capture the global morphology, the colony dimension, the local hyphal distribution and the spatio-temporal evolution of biomass for the growth of *P. placenta*.

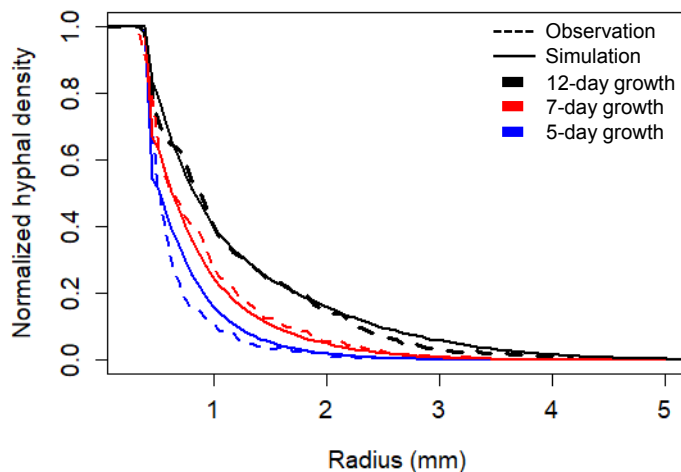


Fig. 6. Evolution of biomass density versus time: observed and simulated density curves at three specific times during the growth period.

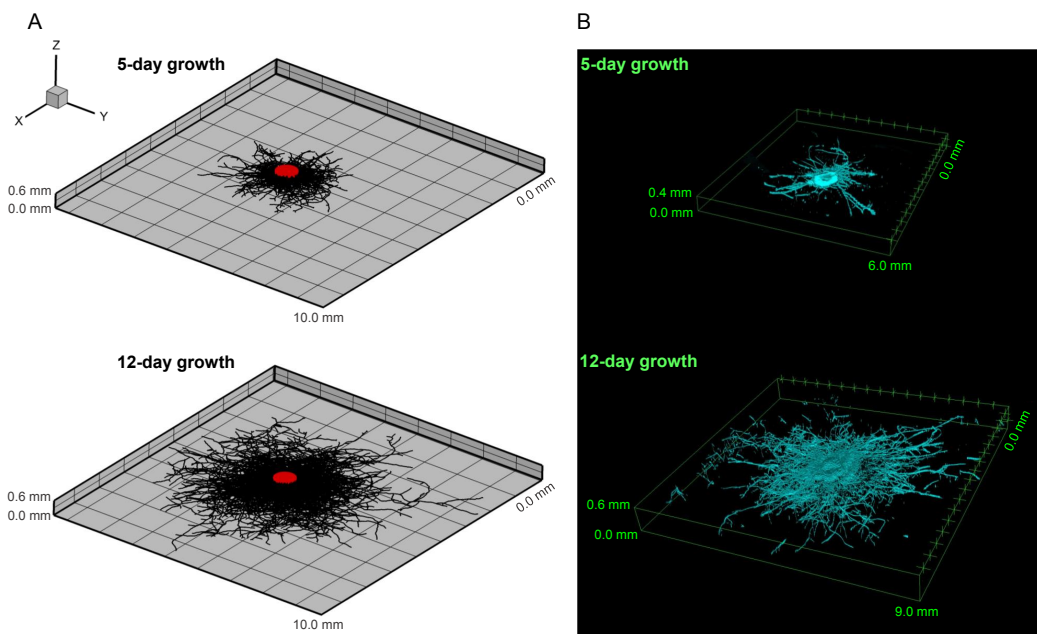


Fig. 7. 3D mycelial networks on agar obtained by the simulation and in the experiment at two specific times during the growth period.

### 345 3.2. Model potential

Generic mechanisms of hyphal growth were incorporated in this model so that it could be easily extended to many other configurations and growth features, such as penetrative hyphae, investigation of hyphal growth in fibrous media or negative

tropisms due to toxicity. Three examples are provided in Fig. 8. Hyphae can penetrate into solid media for absorbing more water and nutrients. The penetrative hyphae tend to grow vertically downward [6] and at an elongation rate reduced by the presence of the solid medium. As shown in Fig. 8(A), the lattice was divided into aerial and substrate parts by the surface at  $z = 0$ . For the substrate part, a penetrative probability  $P_{penetrate}$  was added into the elongation mechanism (Eq. 18) and a constant, downward tropism was applied to the penetrative hyphae. Results show that the penetrative probability can be adjusted to control hyphal penetration rate and hence the number of hyphae penetrated into the medium, while the intensity of tropism greatly influences the penetration direction. These two parameters can be optimized to validate the penetration mechanism.

$$\begin{cases} P_x(i, t) = P_{penetrate} \left[ \frac{\tau}{\delta} R(i, t) \vec{n}(i, t) \cdot \vec{e}_x \right], \\ P_y(i, t) = P_{penetrate} \left[ \frac{\tau}{\delta} R(i, t) \vec{n}(i, t) \cdot \vec{e}_y \right], \\ P_z(i, t) = P_{penetrate} \left[ \frac{\tau}{\delta} R(i, t) \vec{n}(i, t) \cdot \vec{e}_z \right], \\ P_{none}(i, t) = 1 - [P_x(i, t) + P_y(i, t) + P_z(i, t)], \end{cases} \quad (18)$$

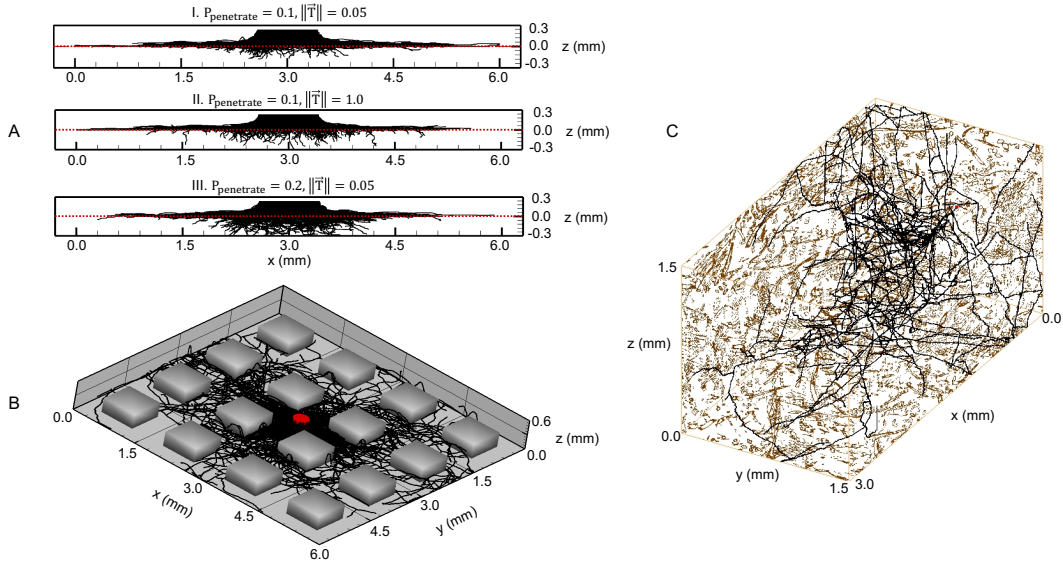


**Fig. 8. Extension of model application.** (A) Hyphal penetration into solid media ( $z \leq 0.0 \text{ mm}$ ) with I  $P_{penetrate} = 0.1$ ,  $\|\vec{T}\| = 0.05$ ; II  $P_{penetrate} = 0.1$ ,  $\|\vec{T}\| = 1.0$ ; III  $P_{penetrate} = 0.2$ ,  $\|\vec{T}\| = 0.05$ . ( $P_{penetrate}$  - penetrative probability of hyphae,  $\|\vec{T}\|$  - intensity of tropism.) (B) Mycelial growth in an obstructed environment: intensity of the thigmotropism  $c_s = 100.0$ . (C) Mycelial growth in a fibreboard from a spore located at  $(x = 0 \mu\text{m}, y = 750 \mu\text{m}, z = 750 \mu\text{m})$ .

Another possible modelling scenario is the mycelial growth in an obstructed environment (Fig. 8(B)). Cuboids of  $0.75 \times 0.75 \times 0.3 \text{ mm}$  were evenly distributed on a surface and the thigmotropism was applied at the surfaces of these cuboids. Hyphae changed their extension direction to pass around the cuboids when they meet an obstacle. Thigmotropism impacted hyphal growth in two ways. When the intensity of

365 the thigmotropism is small, the change rate of the hyphal direction is low, leading to  
a reduction of the elongation rate and hence slightly decreasing the expansion of the  
colony. We also noticed that some hyphae climbed onto the lateral side of the cuboids  
even under the downward tropism since the thigmotropism can also greatly impact  
hyphal elongation direction. If the thigmotropism is high enough, hyphae might  
370 climb onto the cuboids. The experimental observation of the mycelial growth in this  
environment but with different materials for the cuboids is currently in progress to  
develop a better understanding of the interaction of hyphae and obstacles and hence  
to validate this mechanism in the model. The model can also be extended to simu-  
late the mycelial growth in a more complex, fibrous medium (Fig. 8(C)). The real  
375 morphology of a tiny block of fibreboard is visualized and reconstructed using nano-  
tomography and is then incorporated in the cubic lattice. A fungal spore is located  
at the bottom of the block at  $(x = 0 \mu m, y = 750 \mu m, z = 750 \mu m)$  from which  
the mycelium had expanded. The mycelial growth is constrained in the fibreboard  
assuming that the block border is covered by solid materials. Hyphae pass around  
380 the fibres and explore the space gradually from the bottom to the top. A calibration  
experiment is also in progress in our laboratory. Based on the fungal distribution in  
wood, the next step is to incorporate the translocation and degradation mechanisms  
to model fungal decomposition of wood.

#### 4. Conclusion

385 This paper proposes a lattice-based model able to simulate the 3D growth of fungi.  
It includes five fundamental biological mechanisms: hyphal elongation, branching,  
anastomosis, unidirectional tropism and thigmotropism. The 3D model was de-  
veloped from our previous 2D model and therefore inherits its particularity which  
eliminates the restriction of the lattice configuration to hyphal elongation and con-  
390 nection angle while maintaining the simple algorithm and high computing efficiency.  
Therefore, the mycelium generated by this model, even if confined to the lattice, is  
very close to a realistic fungal network. This model was calibrated by experimental  
data on the growth of *Postia placenta* on malt-extracted agar and focuses on the  
investigation of the mycelial growth on a solid medium.

395 The 3D model provides a more realistic representation than the 2D model, both  
in terms of mycelial morphology and biomass density. Indeed, the 3D model involves  
biological mechanisms in a more realistic way and can better reproduce the growth  
environment. As the environment is no longer homogeneous in 3D space, our ob-  
400 jective is to clarify the interactions between hyphae and this environment which is  
heterogeneous in the z-direction. We found that two mechanisms, tropism towards  
the surface and constraint of the emerging branching directions, are essential. The  
tropism intensity should increase rapidly with the distance to the substrate. An  
exponential expression was derived in this work. The constrained branching mech-  
405 anism works particularly well when the tropism is low and very near the substrate  
and its effect is to limit the newly-generated hyphae inside a small band around the

surface.

410 Due to higher computing efficiency (especially RAM but also CPU time) of the  
2D model, it is still useful for modelling superficial growth of fungi. However, the  
3D model is essential for its application to configurations that the 2D model cannot  
handle, such as the penetration of hyphae in a solid medium or growth in a porous  
medium with complex morphology. Therefore, this model can be applied in studying  
415 solid-state fermentation or mycelial growth in wood or fibreboard. Due to the lattice  
structure, the actual wood morphology observed in nano-tomography can be directly  
integrated into our model. In the future, efforts should be made to study degradation  
mechanisms by combining translocation in both directions of experimentation and  
modelling.

## 420 **Acknowledgments**

The calculus presented in this work were performed at the Fusion HPC Center,  
CentraleSupélec, Université Paris-Saclay and the ROMEO HPC Center, Université  
de Reims Champagne-Ardenne. Financial supports from Grand Reims, the Marne  
department and the Grand Est region are gratefully acknowledged.

## 425 **Appendix**

This appendix contains the figure showing the initial field, the simulation geom-  
etry and an example of the simulations.

## **References**

- 430 [1] M. Papagianni, Fungal morphology and metabolite production in submerged  
mycelial processes, *Biotechnol. Adv.* 22 (3) (2004) 189–259. doi:10.1016/j.  
biotechadv.2003.09.005.
- [2] M. Fomina, K. Ritz, G. M. Gadd, Nutritional influence on the ability of fungal  
mycelia to penetrate toxic metal-containing domains, *Mycol. Res.* 107 (July)  
(2003) 861–871. doi:Doi10.1017/S095375620300786x.
- 435 [3] A. Brand, S. Shanks, V. M. S. Duncan, M. Yang, K. Mackenzie, N. A. R. Gow,  
Hyphal orientation of *Candida albicans* is regulated by a calcium-dependent  
mechanism, *Curr. Biol.* 17 (4) (2007) 347–352. doi:10.1016/j.cub.2006.12.  
043.
- 440 [4] T. Crombie, N. A. Gow, G. W. Gooday, Influence of applied electrical fields on  
yeast and hyphal growth of *Candida albicans*, *J. Gen. Microbiol.* 136 (2) (1990)  
311–7.

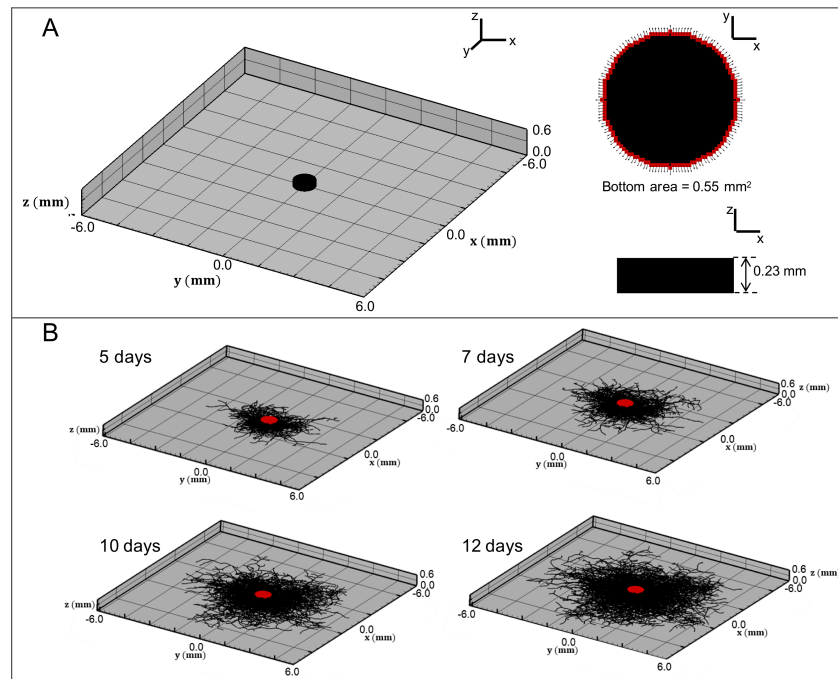


**Fig. A.1.** (A) The initial field of simulations: a cylindrical inoculum of which the lateral border can emerge tips (red points). (B) Simulation results of 4 instants in applying the constrained branching and exponential tropism mechanisms.

- 445 [5] G. Villena, T. Fujikawa, S. Tsuyumu, M. Gutiérrez-Correa, Structural analysis of biofilms and pellets of *Aspergillus niger* by confocal laser scanning microscopy and cryo scanning electron microscopy, *Bioresour. Technol.* 101 (2010) 1920–1926. doi:10.1016/j.biortech.2009.10.036.
- [6] M. Nopharatana, D. Mitchell, T. Howes, Use of confocal scanning laser microscopy to measure the concentrations of aerial and penetrative hyphae during growth of *Rhizopus oligosporus* on a solid surface, *Biotechnol. Bioeng.* 84 (2003) 71–77. doi:10.1002/bit.10752.
- 450 [7] D. Cohen, Computer simulation of biological pattern generation processes, *Nature* 216 (1967) 246–248. doi:https://doi.org/10.1038/216246a0.
- [8] H. Yang, U. Reichl, R. King, E. D. Gilles, Measurement and simulation of the morphological development of filamentous microorganisms, *Biotechnol. Bioeng.* 39 (1) (1992) 44–48. doi:10.1002/bit.260390108.
- 455 [9] A. Meskauskas, L. J. McNulty, D. Moore, Concerted regulation of all hyphal tips generates fungal fruit body structures: experiments with computer visualizations produced by a new mathematical model of hyphal growth., *Mycol. Res.* 108 (April) (2004) 341–353. doi:10.1017/S0953756204009670.

- 460 [10] A. Meskauskas, M. D. Fricker, D. Moore, Simulating colonial growth of fungi with the Neighbour-Sensing model of hyphal growth., *Mycol. Res.* 108 (November) (2004) 1241–1256. doi:10.1017/S0953756204001261.
- [11] I. Carver, G. P. Boswell, A lattice-free model of translocation-induced outgrowth in fungal mycelia, *IAENG Int. J. Appl. Math.* 38 (4) (2008) 173–179.
- 465 [12] M. J. Fuhr, M. Schubert, F. W. M. R. Schwarze, H. J. Herrmann, Modelling the hyphal growth of the wood-decay fungus *Physisporinus vitreus*, *Fungal Biol.* 115 (9) (2011) 919–932. arXiv:1101.1747, doi:10.1016/j.funbio.2011.06.017.
- 470 [13] S. Hopkins, G. P. Boswell, Mycelial response to spatiotemporal nutrient heterogeneity: A velocity-jump mathematical model, *Fungal Ecol.* 5 (2) (2012) 124–136. doi:10.1016/j.funeco.2011.06.006.
- [14] G. Vidal-Diez de Ulzurrun, J. Baetens, J. Van den Bulcke, B. De Baets, Modelling three-dimensional fungal growth in response to environmental stimuli, *J. Theor. Biol.* 414 (2017) 35–49. doi:10.1016/j.jtbi.2016.11.020.
- 475 [15] J. M. Lopez, H. J. Jensen, Nonequilibrium roughening transition in a simple model of fungal growth in 1+1 dimensions, *Phys. Rev. Lett.* 81 (8) (1998) 1734–1737. arXiv:9803171, doi:10.1103/PhysRevLett.81.1734.
- [16] G. P. Boswell, H. Jacobs, K. Ritz, G. M. Gadd, F. A. Davidson, The development of fungal networks in complex environments, *Bull. Math. Biol.* 69 (2007) 605–634. doi:10.1007/s11538-005-9056-6.
- 480 [17] G. Boswell, Modelling mycelial networks in structured environments, *Mycol. Res.* 112 (2008) 1015–1025. doi:10.1016/j.mycres.2008.02.006.
- 485 [18] J. H. Coradin, A. Braun, G. Viccini, L. F. de Lima Luz, N. Krieger, D. A. Mitchell, A three-dimensional discrete lattice-based system for modeling the growth of aerial hyphae of filamentous fungi on solid surfaces: A tool for investigating micro-scale phenomena in solid-state fermentation, *Biochem. Eng. J.* 54 (3) (2011) 164–171. doi:10.1016/j.bej.2011.02.012.
- 490 [19] D. M. D. Smith, J.-P. Onnela, C. F. Lee, M. Fricker, N. F. Johnson, Network Automata: Coupling structure and function in dynamic networks, *Adv. Complex Syst.* 14 (3) (2011) 317–339. arXiv:0701307, doi:10.1142/S0219525911003050.
- [20] M. Manan, C. Webb, Estimation of growth in solid state fermentation: a review, *Malaysian Journal of Microbiology* 14 (2018) 61–69.
- 495 [21] H. Du, P. Lv, M. Ayouz, A. Besserer, P. Perré, Morphological characterization and quantification of the mycelial growth of the Brown-rot fungus *Postia placenta* for modeling purposes, *PLoS One* 11 (9) (2016) e0162469. doi:10.1007/s00253-015-6949-7.

- [22] B. Delahaye, D. Eveillard, N. Bouskill, On the power of uncertainties in microbial system modeling: no need to hide them anymore, *mSystems* 2(6) (2017) e00169–17. doi:10.1128/mSystem.00169-17.
- 500 [23] H. Du, M. Ayouz, P. Lv, P. Perré, A lattice-based system for modeling fungal mycelial growth in complex environments, *Phys. A Stat. Mech. its Appl.* 511 (2018) 191–206. doi:10.1016/j.physa.2018.07.051.
- [24] M. Riquelme, C. G. Reynaga-Peña, G. Gierz, S. Bartnicki-García, What determines growth direction in fungal hyphae?, *Fungal Genet. Biol.* 24 (1-2) (1998) 101–109. doi:10.1006/fgbi.1998.1074.
- 505 [25] M. Riquelme, S. Bartnicki-Garcia, Key differences between lateral and apical branching in hyphae of *Neurospora crassa*, *Fungal Genet. Biol.* 41 (9) (2004) 842–851. doi:10.1016/j.fgb.2004.04.006.
- [26] C. P. Semighini, S. D. Harris, Regulation of apical dominance in *Aspergillus nidulans* hyphae by reactive oxygen species, *Genetics* 179 (4) (2008) 1919–1932. doi:10.1534/genetics.108.089318.
- 510 [27] P. Hickey, D. Jacobson, N. Read, N. Louise Glass, Live-cell imaging of vegetative hyphal fusion in *Neurospora crassa*, *Fungal Genet. Biol.* 37 (2002) 109–119. doi:10.1016/S1087-1845(02)00035-X.
- [28] D. Moore, B. Hock, J. Greening, V. Kern, L. Frazer, J. Monzer, Gravimorphogenesis in agarics, *Mycol. Res.* 100 (3) (1996) 257–273. doi:10.1016/S0953-7562(96)80152-3.
- 515 [29] H. Watts, A. Véry, T. Perera, J. Davies, N. Gow, Thigmotropism and stretch-activated channels in the pathogenic fungus *Candida albicans*, *Microbiology* 144 (Pt 3) (1998) 689–695. doi:10.1099/00221287-144-3-689.
- 520 [30] J. Schumacher, P. Tudzynski, Morphogenesis and pathogenicity in fungi, *Top. Curr. Genet.* 22 (2012) 243–264. doi:10.1007/978-3-642-22916-9.